electrochem

MDPI

Article

Hierarchical Two-Dimensional Layered Nickel Disulfide (NiS_2)@PEDOT:PSS Nanocomposites as Battery-Type Electrodes for Battery-Type Supercapacitors with High Energy Density

Susmi Anna Thomas [1], Jayesh Cherusseri [2,*] and Deepthi N. Rajendran [1,*]

[1] Department of Physics, Government College for Women, University of Kerala, Thiruvananthapuram 695014, Kerala, India; susmithomas123@gmail.com

[2] School of Engineering and Technology, Sunway University, No. 5, Jalan Universiti, Bandar Sunway 47500, Selangor Darul Ehsan, Malaysia

* Correspondence: jayeshc@sunway.edu.my or drjayeshpuli@gmail.com (J.C.); deepthinrphysics@gmail.com (D.N.R.)

Abstract: Battery-type hybrid supercapacitors (HSCs) (otherwise known as supercapatteries) are novel electrochemical energy storage devices bridge the gap between rechargeable batteries and traditional SCs. Herein, we report the synthesis of layered two-dimensional (2D) nickel disulfide (NiS_2) nanosheets (NSNs) modified with poly(3,4-ethylenedioxythiophene:polystyrene sulfonate (PEDOT:PSS) and their successful implementation in battery-type SCs. Initially, a layered 2D NSN is synthesized via a microwave-assisted hydrothermal method and further used as a template to coat PEDOT:PSS in order to prepare NiS_2@PEDOT:PSS nanocomposite electrodes by a facile drop-casting method. This is the first-time report on the synthesis of a hierarchical NiS_2@PEDOT:PSS nanocomposite electrode for battery-type HSC applications. An asymmetric battery-type HSC fabricated with NSN@PEDOT:PSS nanocomposite as positrode and activated carbon as negatrode delivers a maximum energy density of 52.1 Wh/kg at a current density of 1.6 A/g with a corresponding power density of 2500 W/kg.

Keywords: nickel disulfide; supercapacitor; PEDOT:PSS; nanocomposite electrode; battery-type hybrid; microwave-assisted hydrothermal

Citation: Thomas, S.A.; Cherusseri, J.; Rajendran, D.N. Hierarchical Two-Dimensional Layered Nickel Disulfide (NiS_2)@PEDOT:PSS Nanocomposites as Battery-Type Electrodes for Battery-Type Supercapacitors with High Energy Density. *Electrochem* **2024**, *5*, 298–313. https://doi.org/10.3390/electrochem5030019

Academic Editor: Masato Sone

Received: 10 May 2024
Revised: 1 July 2024
Accepted: 11 July 2024
Published: 17 July 2024

1. Introduction

In comparison to traditional SCs, the prominent advancement in electronics with smart technology demands energy storage systems with higher reliability and prominent efficiency [1]. Among the various available energy storage devices, the SC is a highly efficient renewable and sustainable energy resource which possesses higher charge-discharge capability, long cycle life, and higher density [2,3]. The SC is an ideal candidate for flexible device fabrication due to its simple structure, inherent electrochemical feature and feasible production. According to the mechanism of energy storage, SCs are classified mainly into two categories: electrochemical double layer capacitors (EDLCs) and pseudocapacitors [4,5]. For an EDLC, the charges are stored through reversible adsorption/desorption of electrolyte ions present in the electrode/electrolyte. Pseudocapacitor store charges by rapid surface redox reaction [6,7]. The electrodes which act as an EDLC are of carbonaceous material. On the other hand, there exists a disadvantage due to the reduced energy density of SCs in comparison to a rechargeable battery, and it does not satisfy the demand for higher energy [2,8]. The major factor which affects the performance of SCs is selection of electrode materials; it holds higher electrical conductivity to promote rapid charge-discharge [9,10]. There are different types of electrode materials such as carbon, conducting polymer, and transition metal oxide/hydroxides which are utilized as active material for SC fabrication [11–13]. But these materials have their own disadvantages due to the reduced specific

capacitance value of carbon materials, low cycling stability of the conducting polymer, and the smaller value of conductivity possessed by transition metal oxide/hydroxides [14].

Among these different types of electrode materials, transition metal sulfides have attracted prominent research interest due to their higher theoretical capacity, reduced cost, and environmental friendliness [15]. Currently, transition metal sulfides including nickel sulfide (NiS, Ni_3S_2), cobalt sulfide (CoS, Co_3S_4), and ternary nickel cobalt sulfide ($NiCo_2S_4$, $Ni_xCo_{3-x}S_4$) are extensively evaluated as electrode materials for SC device fabrication due to their intrinsic physical properties and unique structural pattern [16]. Among these electrodes, NiS_2 is a potential electrode for SCs due to its redox reaction in metal ions, reduced cost, natural abundance, higher conductivity, and environmental benignity compared to other transition metal oxides. Nickel sulfide is found in many different forms like NiS, NiS_2, β-Ni_3S_2, α-$Ni_{3+x}S_2$, Ni_4S_{3+x}, Ni_6S_5, Ni_7S_6, Ni_9S_8, and Ni_3S_4 which possess nanoflakes or hollow nanospheres. Nickel sulfide forms improve electrochemical characteristics, higher capacitance capability, and stability [17,18]. These proposed studies introduced the efficiency of nickel disulfide with nano/micro structural features to depict it as promising solution to increase characteristics such as reduced density, surface permeability, reduced electron/ion transport pathway, and perfectly defined interior voids. Thereby, it is very important to explore the possibility of the utilization of nickel sulfide as a promising electrode material for SC device fabrication. In addition to these advantages, NiS_2 is efficient with respect to three major benefits. The first is their reduced charge transfer resistance, and the second is the higher electronegativity of oxygen in comparison to sulfur, which improves electron transport exists in the structure [19]. Finally, the oxygen replacement with sulfur in the resultant material contributes to the preparation of nanomaterials like nanospheres, nanocubes, and nanosheets. Consequently, nickel sulfides have reduced charge transfer resistance due to the influence of electron transfer rate and their lower bandgap value of about 0.5 eV in comparison to Cu_xS_y (2.1 eV). Nickel sulfide is a class of semiconductor having variety of compositions illustrated in different fields such as dye-sensitized solar cells, hydrogen evolution, etc. [20].

NiS_2-based electrodes found application in SCs with higher performance. The practical application of NiS_2 electrodes is limited by base carrier usage and easier damage of structure during redox reactions, which have prominent research interest for their modification [21]. An efficient way to modify the performance of nickel sulfide is by the addition of various additives like conducting polymers, carbonaceous polymers, etc., which are able to store charges entirely in the body having rapid charge-discharge kinetics due to their efficient conductivity [19]. Their poor cycling stability and mechanical ability reduces their widespread application in pseudocapacitors. The conducting polymers, like poly(3,4-ethylenedioxythiophene)/poly(strenesulfonate) (PEDOT:PSS), polyaniline, polypyrrole, etc., are promising candidates to avoid its reduction in performance through synergistic interaction between individual components [22]. Among these, PEDOT:PSS is a promising polymer, which makes easier combination with metal sulfides in accordance with their higher conductivity, faster redox reaction, feasible processability, and efficient electrochemical stability. PEDOT:PSS is a highly efficient film which offers higher flexibility to SC device fabrication for practical applications [23]. There is a report based on a one-pot hydrothermal approach for the synthesis of solution-processable MoS_2/PEDOT:PSS by direct treatment from a solution consisting of Na_2MoO_4, L-cysteine, and PEDOT:PSS. The proposed composite hydrogels are able to execute easier dispersion in water to prepare stable dispersion to utilize them as an ink for 3D printing and to fabricate free-standing MoS_2/PEDOT:PSS flexible films by vacuum filtration. A sheet-like architecture is obtained for prepared composite film with uniform distribution of elements. In aqueous Na_2SO_4 electrolyte, the film having 34.8% MoS_2 delivers a higher capacitance value of 474 mF/cm^2 at 0.5 mA/cm^2 current density. Also, the composite film has an efficient rate capability of 240 mF/cm^2 at 8 mA/cm^2 and capacity retention of 224 mF/cm^2 at 4 mA/cm^2 after 5000 cycles. Robustness and flexibility of the assembled device is demonstrated through

higher capacitance retention of 94 and 89% obtained for the prepared film after bending it to 180° for 5000 cycles for aqueous and solid-state electrolytes, respectively [24].

The present work deals with the synthesis of nanocomposites comprising PEDOT:PSS-modified NiS_2 nanosheets and their electrochemical performance evaluation in order to use them as electrode-active materials for battery-type SCs. Initially, the NiS_2 nanosheet is synthesized by microwave-assisted hydrothermal method which is adopted to synthesize a NiS_2/PEDOT:PSS nanocomposite SC electrode. Further, the influence of PEDOT:PSS on the electrochemical performance of NiS_2 nanosheets is evaluated. In the case of a conventional hydrothermal approach, it is difficult to monitor the reaction parameters such as pressure, temperature, etc. [5]. Therefore, it is difficult to achieve homogeneous nucleation of particles, which in turn has a negative impact on electrochemical cycling stability when used an electrode-active material for SCs. This issue can be resolved by adopting the microwave-assisted hydrothermal method for the synthesis of nanomaterials whereby control of heating rate, temperature, and pressure to the reaction vessel can be achieved. This helps in inducing a homogeneous nucleation of the resultant material and proceeded with the growth of material with a uniform size and shape. The NiS_2/PEDOT:PSS nanocomposite SC electrodes are prepared by varying the mass concentration of NiS_2 and PEDOT:PSS. The charge storage mechanism of NiS_2/PEDOT:PSS nanocomposite SC electrodes is evaluated by Dunn's kinetic method and found to exhibit a battery-type charge storage. Among the various 2D NSN/PEDOT:PSS nanocomposite SC electrodes, NPS1 exhibits a higher area under the CV curve, which exhibits a superior charge storage performance when compared to the others. A mass specific capacity of 462.57 C/g is obtained at a scan rate of 10 mV/s for the NPS1 nanocomposite SC electrode. The synergistic interaction between NiS_2 and PEDOT:PSS introduced an efficient battery-type SC electrode character to the NPS1 nanocomposite SC electrode.

2. Experimental Section

2.1. Chemicals and Materials

Nickel nitrate hexahydrate ($Ni(NO_3)_2.6H_2O$; 99%), thiourea (CH_4N_2S; 99%), polyvinylidene difluoride (PVDF), carbon black, PEDOT:PSS, and N-methyl-2-pyrrolidone (NMP) (C_5H_9NO; 99%) were purchased from Sigma-Aldrich (M) Sdn. Bhd., Malaysia. Deionized water was used for the microwave hydrothermal synthesis of 2D NSNs.

2.2. Synthesis of NSN/PEDOT:PSS Nanocomposites

The microwave-assisted hydrothermal method of synthesizing 2D NSNs was adopted to prepare 2D NSN/PEDOT:PSS nanocomposite SC electrodes in accordance with our earlier published work [25]. The battery-type SC electrodes were prepared by coating the material over nickel foam substrate to promote the electronic conductivity. An amount of 1 mg/mL PEDOT:PSS solution was dispersed in 3 mg of 2D NSN in order to prepare the SC electrode and sonicated to achieve a well-defined suspension. The electrodes for battery-type SCs were prepared by slurry casting over nickel foam and no polymeric or other type of binder was used. The as-prepared electrode is labelled as NPS1. The geometrical area of the SC electrode was fixed to 1 cm^2. The mass of electrode-active material was fixed to 3 mg in a SC electrode. The same procedure was repeated by changing PEDOT:PSS to 3 mg/mL and 5 mg/mL which were labelled as NPS2 and NPS3, respectively. All the nanocomposite samples were dried in an oven kept at 60 °C overnight. A schematic diagram representing the synthesis of 2D NSN/PEDOT:PSS nanocomposite is provided in Scheme 1.

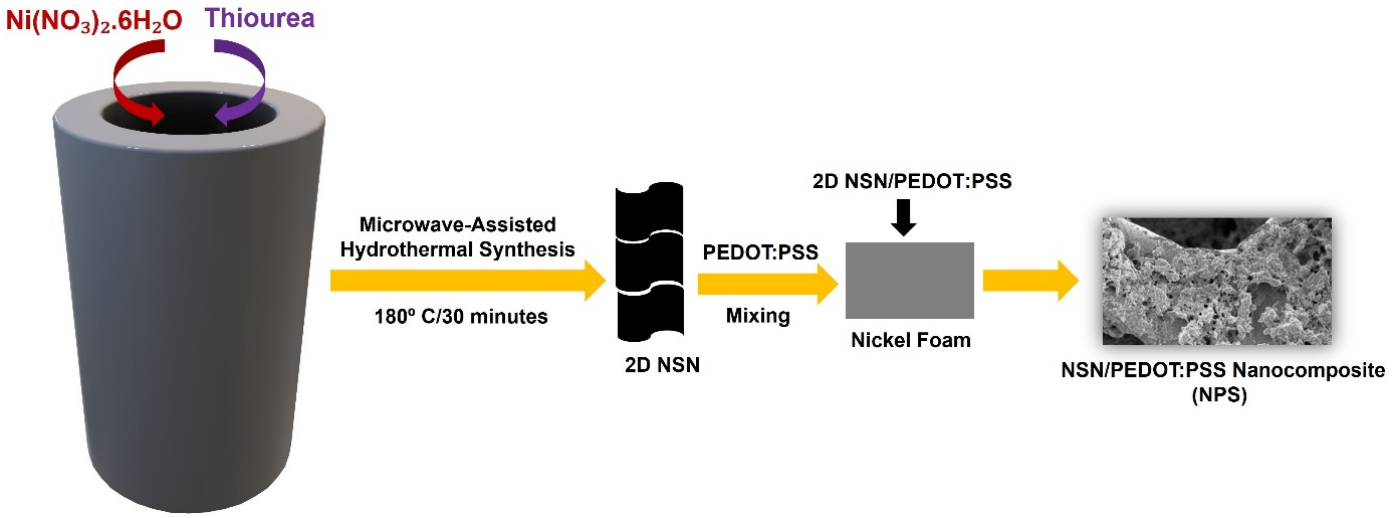

Scheme 1. Schematic diagram of the preparation of NSN/PEDOT:PSS nanocomposite.

2.3. Material Characterizations of NSN/PEDOT:PSS Nanocomposites

The microstructure and surface morphology of microwave hydrothermally-synthesized 2D NSN and 2D NSN/PEDOT:PSS nanocomposite were examined using FESEM imaging. The mass of samples was measured using a high-precision microbalance with a readability of 10 μg.

2.4. Electrochemical Characterizations of NSN/PEDOT:PSS Nanocomposites

The electrochemical performance of the 2D NSN/PEDOT:PSS nanocomposite SC electrodes was examined by EIS, CV, and GCD measurements. The CV analysis was performed within a potential window of 0 V to 0.6 V at different scan rates, such as 100 mV/s, 80 mV/s, 60 mV/s, 40 mV/s, 20 mV/s, and 10 mV/s. The EIS analysis was carried out within a frequency range of 10^5 Hz to 0.01 Hz. The 2D NSN/PEDOT:PSS nanocomposite SC electrodes were tested in a three-electrode cell configuration by using 2D NSN/PEDOT:PSS nanocomposite as working electrode, platinum as counter electrode, and SCE as reference electrode. All the electrochemical characterizations were carried out using 2 M KOH (aqueous) electrolyte. The electrochemical performance of the electrodes was also tested in a two-electrode cell configuration.

3. Results and Discussion

3.1. Microstructure and Surface Morphology of NPS1 Nanocomposite

The microstructure and surface morphology of the 2D NSN was examined using FESEM imaging and Figure 1a–c represent the FESEM images of the 2D NSN at three different magnifications. From these images, it can be observed that the 2D NSN exhibits a flake-like fluffy structure, as discussed in our earlier work [25]. The EDX elemental mapping images to show the distribution of nickel and sulfur in the 2D NSN are shown in Figure 1d,e, respectively. This confirms the presence of nickel and sulfur in the 2D NSN. The FESEM images of the 2D NSN/PEDOT:PSS (NPS1) nanocomposite SC electrode are shown in Figure 1f,g. This particular nanocomposite combination, NPS1, exhibits a superior electrochemical performance when used as an SC electrode, which will be discussed at a later stage. The 2D NSN mixed with PEDOT:PSS coated over nickel foam shows an open porous network structure, which is highly beneficial in attaining good electrochemical performance when used as electrode-active materials in SCs.

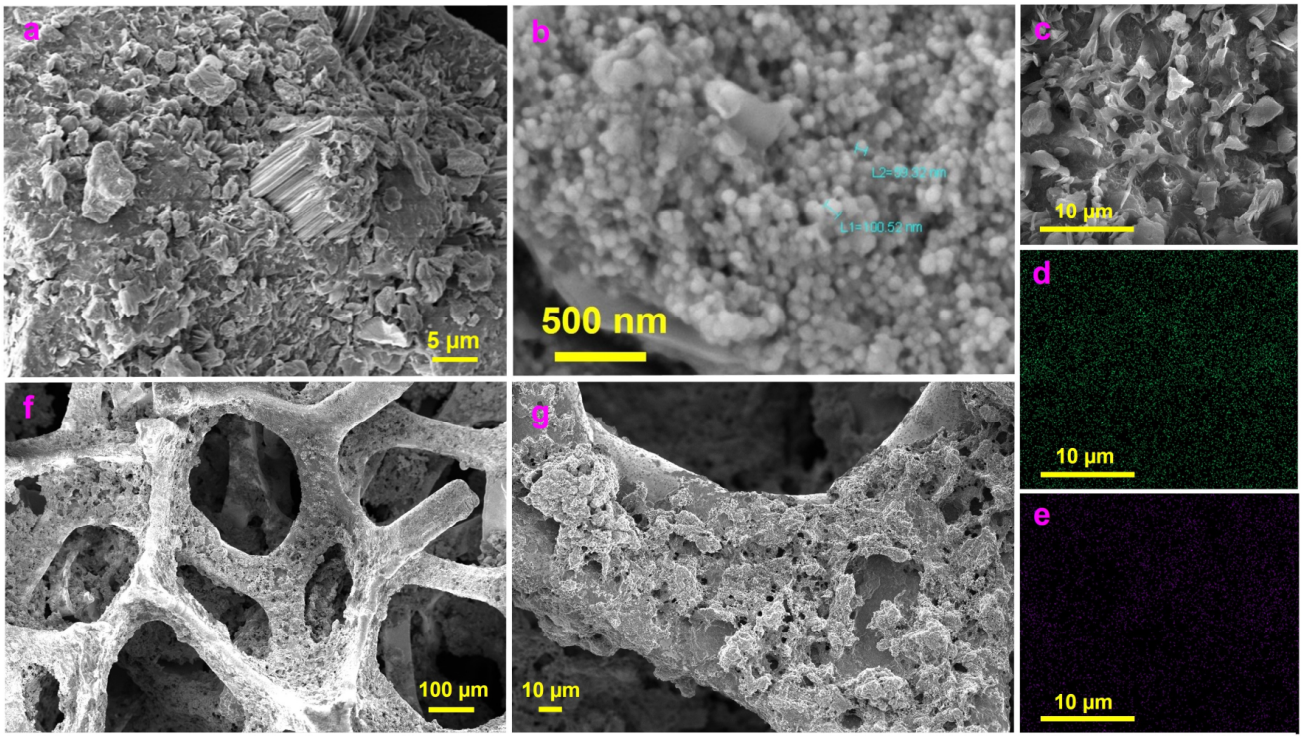

Figure 1. (**a**–**c**) FESEM images of 2D NSN and the corresponding EDX mapping images for (**d**) nickel and (**e**) sulfur; (**f**,**g**) FESEM images of NPS1 nanocomposite SC electrode.

3.2. Electrochemical Performance Evaluation of NSN/PEDOT:PSS Nanocomposites

The electrochemical performance characteristics of the PEDOT:PSS-modified 2D NSN electrodes was evaluated in a three-electrode cell configuration in 2 M KOH (aqueous) electrolyte. The EIS analysis represented in the form of a Nyquist plot obtained for the pristine PEDOT:PSS SC electrode is shown in Figure 2a,c and those for the 2D NSN/PEDOT:PSS nanocomposite SC electrodes are shown in Figure 2b,d–h. A Nyquist plot is the representation of the real and imaginary parts of impedance within a specified frequency range. The Nyquist plot of the PEDOT:PSS SC and 2D NSN/PEDOT:PSS nanocomposite SC electrodes contains three regions: the high-frequency region contains a semi-circle, the high-medium frequency region contains a straight line with a slope of ~45°, and the low-frequency contains a vertical line parallel to the *Y*-axis.

From the low-frequency region, the series resistance to the SC electrodes can be estimated. An ideal SC character can be visualized from the Nyquist plot at low-frequency region. In the case of the PEDOT:PSS SC electrode and 2D NSN/PEDOT:PSS nanocomposite SC electrodes, a deviation from this behavior can be seen, which shows the non-capacitive nature of the SC electrodes. The type of charge storage in the 2D NSN/PEDOT:PSS nanocomposite SC electrodes is estimated by Dunn's kinetic method and will be discussed at a later stage. The EIS spectra analysis using Nyquist plots with ZSimpWin software version 3.2 delivers a series resistance of 0.41 Ω, 0.39 Ω, 0.33 Ω, and 0.30 Ω for the pristine PEDOT:PSS SC electrode and the NPS1, NPS2, and NPS3 nanocomposite SC electrodes, respectively.

From the EIS analysis, it is clear that NPS1 exhibits a lowest series resistance when compared with the other SC electrodes. To evaluate the charge storage exhibited by the SC electrodes, CV analysis was performed within a potential window of 0–0.6 V at different scan rates and the results are shown in Figure 3a–d. The CV curves of the pristine PEDOT:PSS SC electrode (Figure 3a) and the NSN/PEDOT:PSS nanocomposite SC electrodes (Figure 3b–d) exhibit a pseudocapacitive charge storage that arises from the redox reactions. The CV profiles consist of oxidation and reduction peaks, representing an anodic peak with positive current density and a cathodic peak with negative current density. The appearance of redox peak pairs in the CV curves of the 2D NSN/PEDOT:PSS

nanocomposite SC electrodes shows that the charge storage is mainly by means of redox reactions. The cathodic peak in the CV curve is introduced by the K^+-ion insertion into the 2D layered NiS_2 architecture, modified with PEDOT:PSS. A high symmetry to the CV curves shows an excellent electrochemical stability held by the SC electrodes.

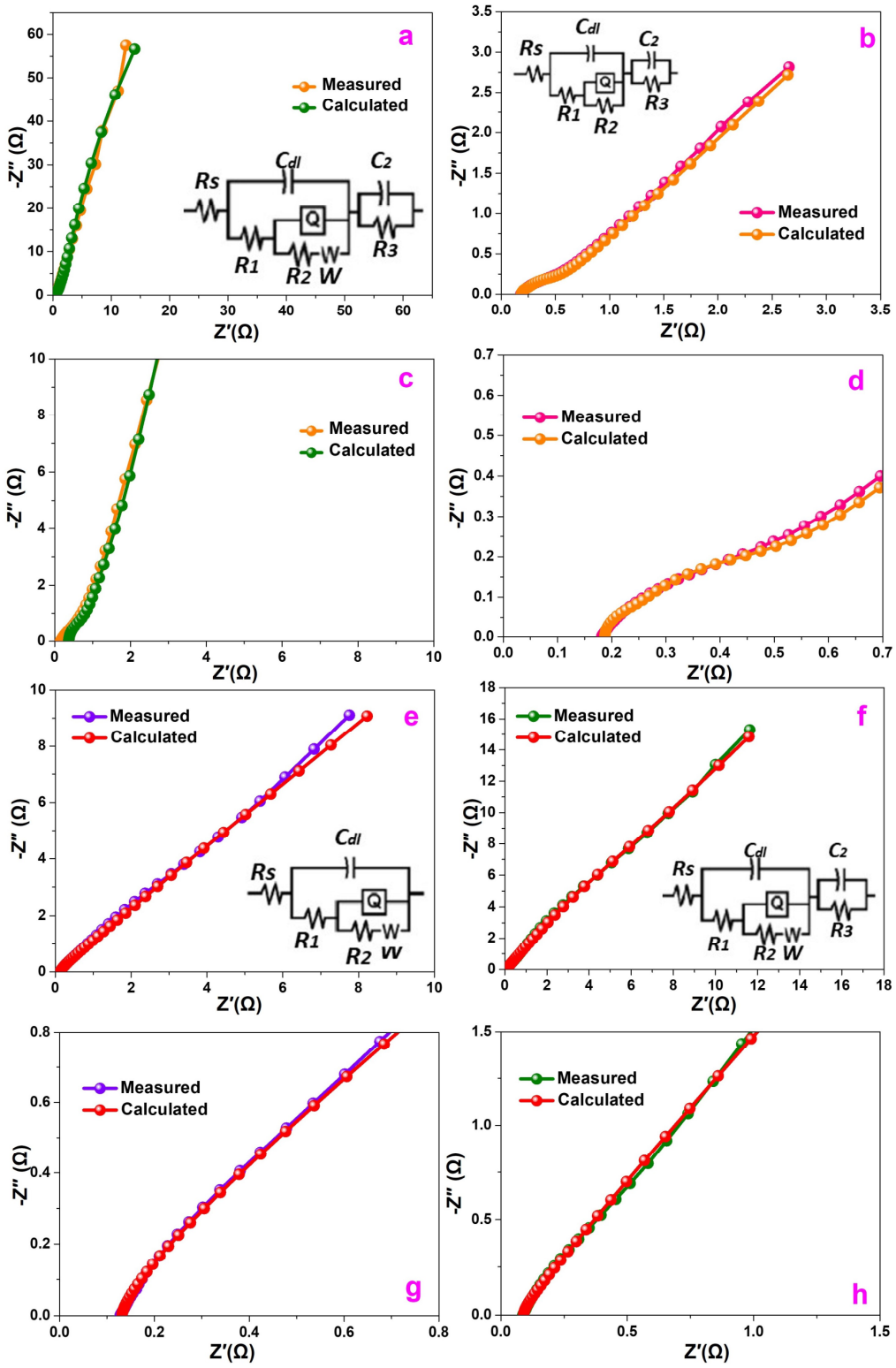

Figure 2. Nyquist plots of (**a**) pristine PEDOT:PSS SC electrode and (**b**) NPS1, (**e**) NPS2, (**f**) NPS3 nanocomposite SC electrodes. Nyquist plot in high-frequency region of (**c**) pristine PEDOT:PSS SC electrode and (**d**) NPS1, (**g**) NPS2, (**h**) NPS3 nanocomposite SC electrodes.

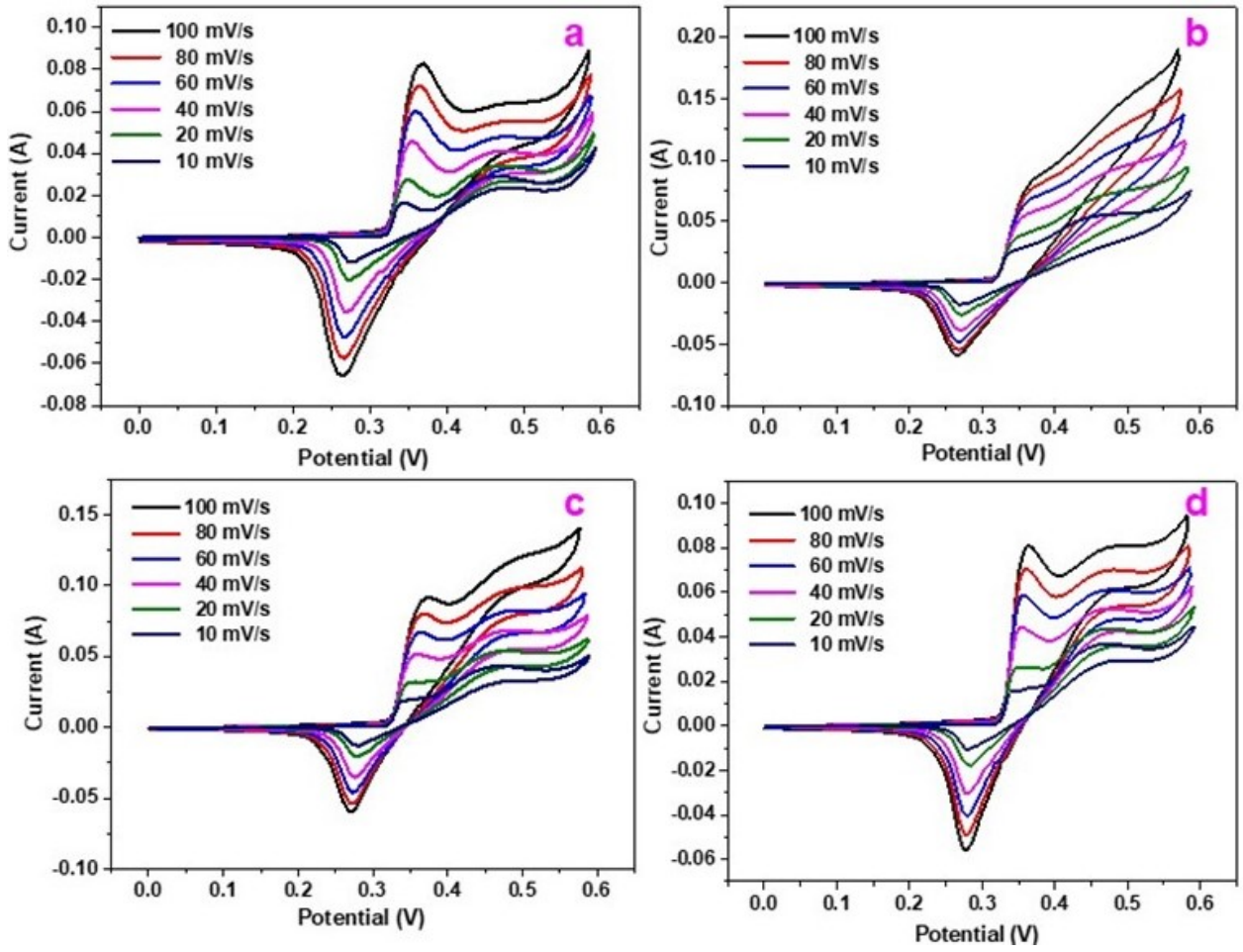

Figure 3. CV curves obtained at different scan rates of (**a**) pristine PEDOT:PSS SC electrode and (**b**) NPS1, (**c**) NPS2, (**d**) NPS3 nanocomposite SC electrodes.

With respect to an increase in scan rate, there exists an increase in redox current, which tends to produce anodic peak shift towards a positive potential and cathodic peak towards a negative potential. Even at higher scan rates, the shape of the CV curves possesses no significant variation, which shows the excellent electrochemical reversibility and rate performance of the SC electrode. The area under a CV curve of the 2D NSN/PEDOT:PSS nanocomposite SC electrodes indicates their charge storage performance and a CV curve with a higher area under the curve exhibits superior performance. Among the various 2D NSN/PEDOT:PSS nanocomposite SC electrodes, NPS1 exhibits a higher area under the CV curve, which exhibits a superior charge storage performance when compared to the others. A mass specific capacity of 462.57 C/g is obtained at a scan rate of 10 mV/s for the NPS1 nanocomposite SC electrode. The synergistic interaction between NiS_2 and PEDOT:PSS introduced an efficient battery-type SC electrode character to NPS1 nanocomposite SC electrode. The GCD analyses of the pristine PEDOT:PSS SC electrode and the NSN/PEDOT:PSS nanocomposite SC electrodes are given in Figure 4a–d. From the GCD curves, it can be observed that the initial and final portions correspond to an EDLC behavior.

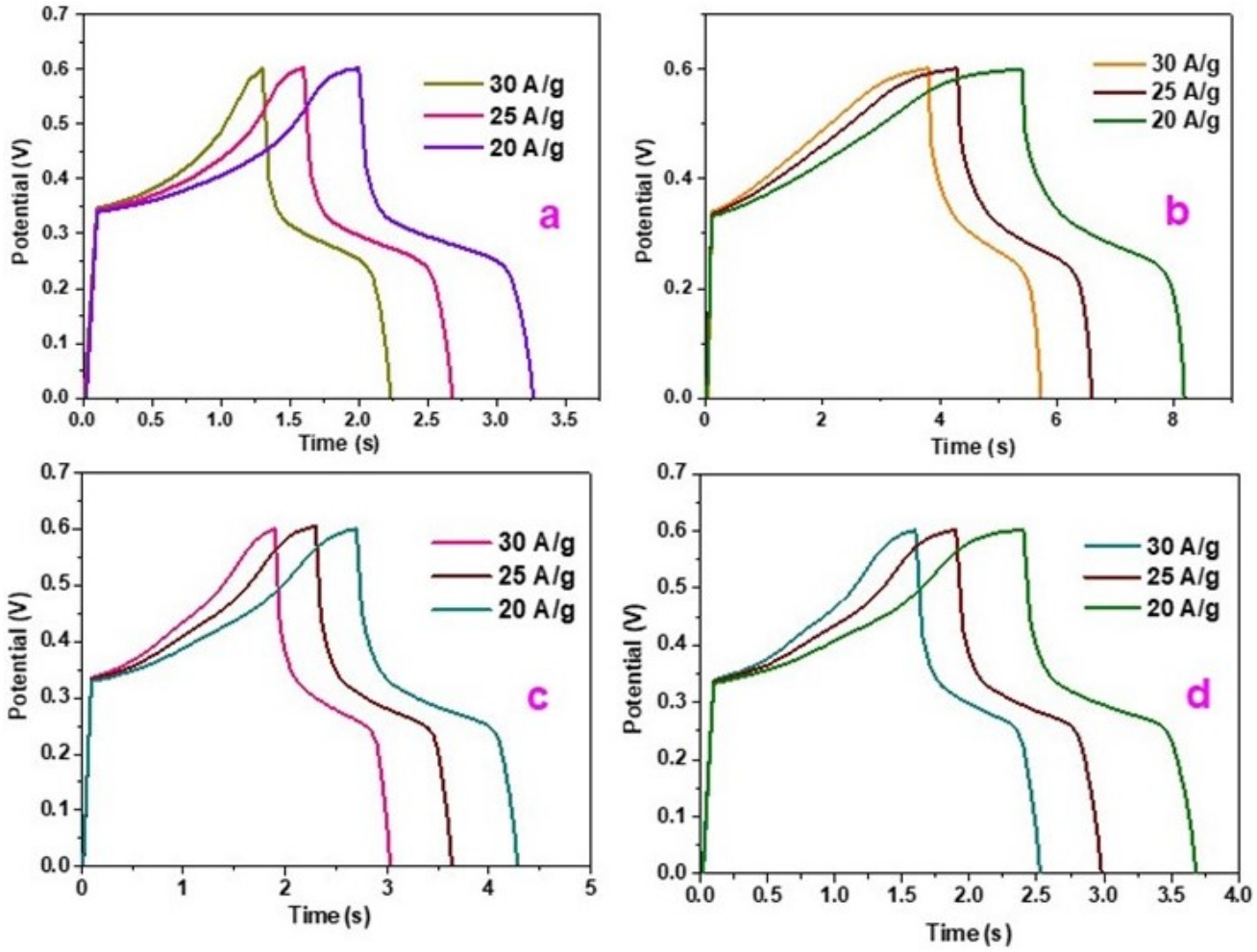

Figure 4. GCD curves obtained at different current densities of (**a**) pristine PEDOT:PSS SC electrode and (**b**) NPS1, (**c**) NPS2, (**d**) NPS3 nanocomposite SC electrodes.

The solvated ions intercalation and faradaic reaction in the final portion correspond to a battery-type charge storage behavior. Thus, the proposed PEDOT:PSS-modified NiS_2 electrodes are said to exhibit a battery-type character, which is confirmed using Dunn's kinetic method and will be discussed later. At higher current densities, the charge-discharge performance of the NSN/PEDOT:PSS nanocomposite SC electrodes is found to be diminished. The plots showing the variation in the mass specific capacity with respect to scan rate for the pristine PEDOT:PSS SC electrode and the NSN/PEDOT:PSS nanocomposite SC electrodes are depicted in Figure 5a–d. The pristine PEDOT:PSS SC electrode delivers a mass specific capacity of 162.87 C/g at a scan rate of 10 mV/s. The NSN/PEDOT:PSS nanocomposite SC electrodes, such as NPS1, NPS2, and NPS3, exhibit a mass specific capacity of 462.57 C/g, 234.4 C/g, and 185.54 C/g, respectively, at a scan rate of 10 mV/s. The area specific capacities of the pristine PEDOT:PSS SC electrode and the NSN/PEDOT:PSS nanocomposite SC electrodes are given in Figure 6a–d. The NPS1 SC electrode also exhibits an area specific capacity of 2.77 C/cm^2 at 10 mV/s, which reveals the efficiency of this optimized electrode for further studies.

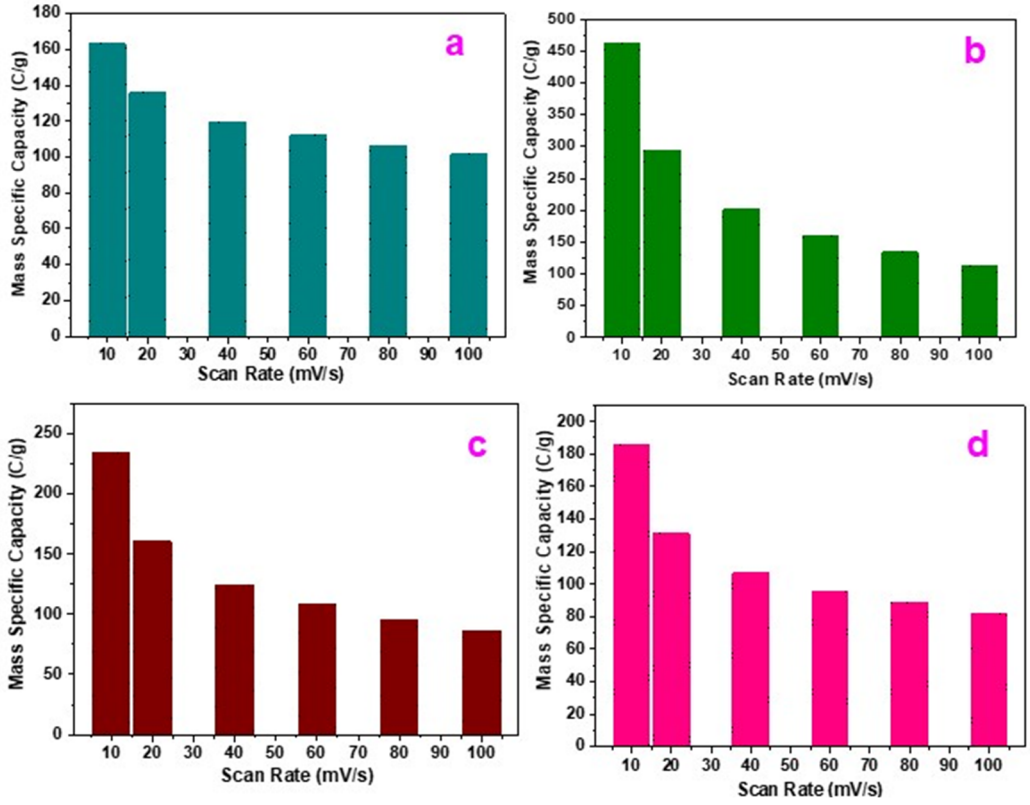

Figure 5. Plot of variation in the mass specific capacity at different scan rates for (**a**) pristine PEDOT:PSS SC electrode and (**b**) NPS1, (**c**) NPS2, (**d**) NPS3 nanocomposite SC electrodes.

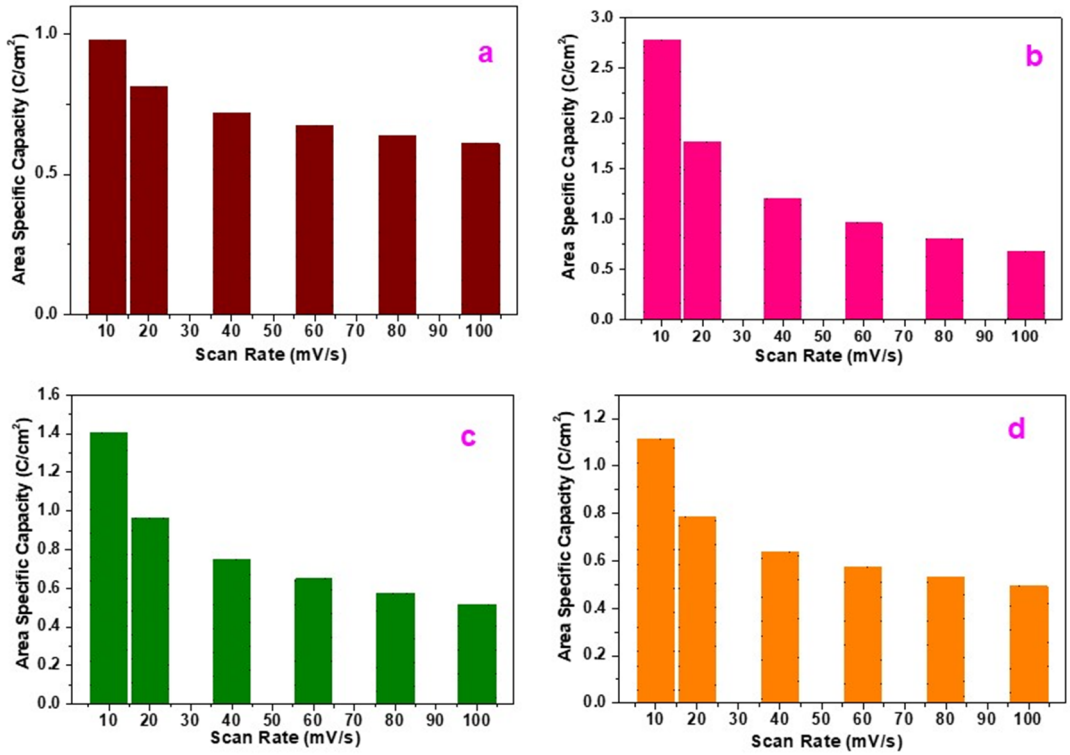

Figure 6. Calculation of area specific capacity in C/cm^2 for (**a**) pristine PEDOT:PSS SC electrode and (**b**) NPS1, (**c**) NPS2, (**d**) NPS3 nanocomposite SC electrodes.

A reduction in the specific capacity with respect to an increase in scan rate can be observed, which is a clear indication of battery-type storage behavior of the electrode-active material. At lower scan rates, the electrolyte ions have enough time to penetrate through the open pores of PEDOT:PSS-modified NiS_2 electrode, but at higher scan rates, there is a chance for redox reactions at the surface/near the surface since the electrolyte ions do not have sufficient time to diffuse through the inner pores of the electrode-active material. This behavior can be seen in the case of the pristine PEDOT:PSS SC electrode as well as the NSN/PEDOT:PSS nanocomposite SC electrodes. When the concentration of PEDOT:PSS in the nanocomposite is increased, there is a reduction in mass specific capacity as well as in area specific capacity. This may be due to the change in the electrode nanostructure with a less open pore structure. This eventually restricts the ability of the electrolyte ions to penetrate through the pores. The optimum concentration of PEDOT:PSS in the NPS1 nanocomposite SC electrode provides an open porous electrode nanostructure, which helps in maximizing the available electrochemical surface area for an enhanced redox reaction to occur. With an increase in the concentration of PEDOT:PSS, there is a reduction in the diffusion rate of electrolyte and a limitation in the charge transfer rate, which eventually deteriorates the performance. Since the NPS1 nanocomposite SC electrode exhibits superior performance, it is used for further studies. To differentiate the types of charge storage possessed by the NPS1 SC electrode, Dunn's kinetic method was adopted.

The anodic and cathodic peak processes deduced from the CV analysis for the NPS1 nanocomposite SC electrode are given by a graphical representation of $log\ i$ and $log\ v$, as shown in Figure 7a,b, respectively. A mean value of cathodic and anodic peak 'b' is about 0.47, which relates to the diffusion-controlled character of NPS1 SC electrode; thus, this electrode is proven to be a battery type. The CV curves of the NPS1 nanocomposite SC electrode displayed in Figure 7c exhibit a capacitive (surface-controlled) contribution (shaded with green), which is about 9.28% of overall specific capacity determined at a scan rate of 40 mV/s, but the contribution introduced from the diffusion-controlled process (shaded with orange) is about 90.72%. The battery-type (diffusion-controlled) total charges stored by the NPS1 nanocomposite SC electrode at various scan rates of 100 mV/s, 80 mV/s, 60 mV/s, 40 mV/s, 20 mV/s, and 10 mV/s are 85.88%, 86.21%, 89.23%, 90.72%, 92.14%, and 94.42%, respectively (Figure 7d). A higher diffusion-controlled phenomenon in the NPS1 SC electrode makes it an efficient battery-type material. The cycling stability of the NPS1 nanocomposite SC electrode was examined in 2 M KOH (aqueous) electrolyte at a constant scan rate of 40 mV/s for 5000 cycles. The variation in the mass specific capacity at different cycle numbers is shown in Figure 8a. A capacity retention of 90.11% is obtained even after completing 5000 cycles (Figure 8b).

3.3. Electrochemical Performance Evaluation of NPS1/PEDOT:PSS//AC HSC Cell

To meet the requirements of practical applications, a battery-type HSC cell was assembled using NPS1 as positrode and AC as negatrode. The operating potential window for the AC and NPS1 nanocomposite SC electrode lies within a range of −1–0 V and 0–0.6 V, respectively, as shown in Figure 9a. The operating potential window for the battery-type NPS1//AC HSC cell is fixed as 0–1.5 V. As shown in Figure 9b, CV analysis was performed for battery-type NPS1//AC HSC cell at different scan rates. With an increase in scan rate, the shape of the CV curves remains unaltered. Figure 9c represents the GCD curves of the battery-type NPS1//AC HSC cell obtained at different current densities. The GCD curves possess typical battery-type behavior, as discussed previously. The calculation of mass specific capacity and area specific capacity of the battery-type NPS1//AC HSC cell is calculated at different current densities. The Nyquist plot obtained for the battery-type NPS1//AC HSC cell is given in Figure 9d. Similar to the three-electrode cell results, the Nyquist plot shows a shift from ideal SC behavior; hence this result agrees that the prepared NPS1 is a battery type. The Nyquist plot of the battery-type NPS1//AC HSC cell in the high-frequency region along with an equivalent circuit model are given as inset images in Figure 9d. The series resistance of the cell was evaluated with an equivalent circuit

model and a series resistance of 3.17 Ω was observed. Figure 10a shows the mass specific capacity variation with respect to different current densities. The maximum mass specific capacity obtained for the battery-type NPS1//AC HSC cell is 250.5 C/g at a current density of 1.6 A/g. Figure 10b represents the variation in area specific capacity of the battery-type NPS1//AC HSC cell at different current densities. A higher area specific capacity of 3 C/cm^2 is obtained for the battery-type NPS1//AC HSC cell at a current density of 1.6 A/g. The variation in the mass specific energy density of the battery-type NPS1//AC HSC cell at different current densities is depicted in Figure 10c. The battery-type NPS1//AC HSC cell exhibits a maximum mass specific energy density of about 52.18 Wh/kg at a current density of 1.6 A/g. The area specific energy density is an important criterion, which demonstrates the practical application of the HSC cell for planar device applications.

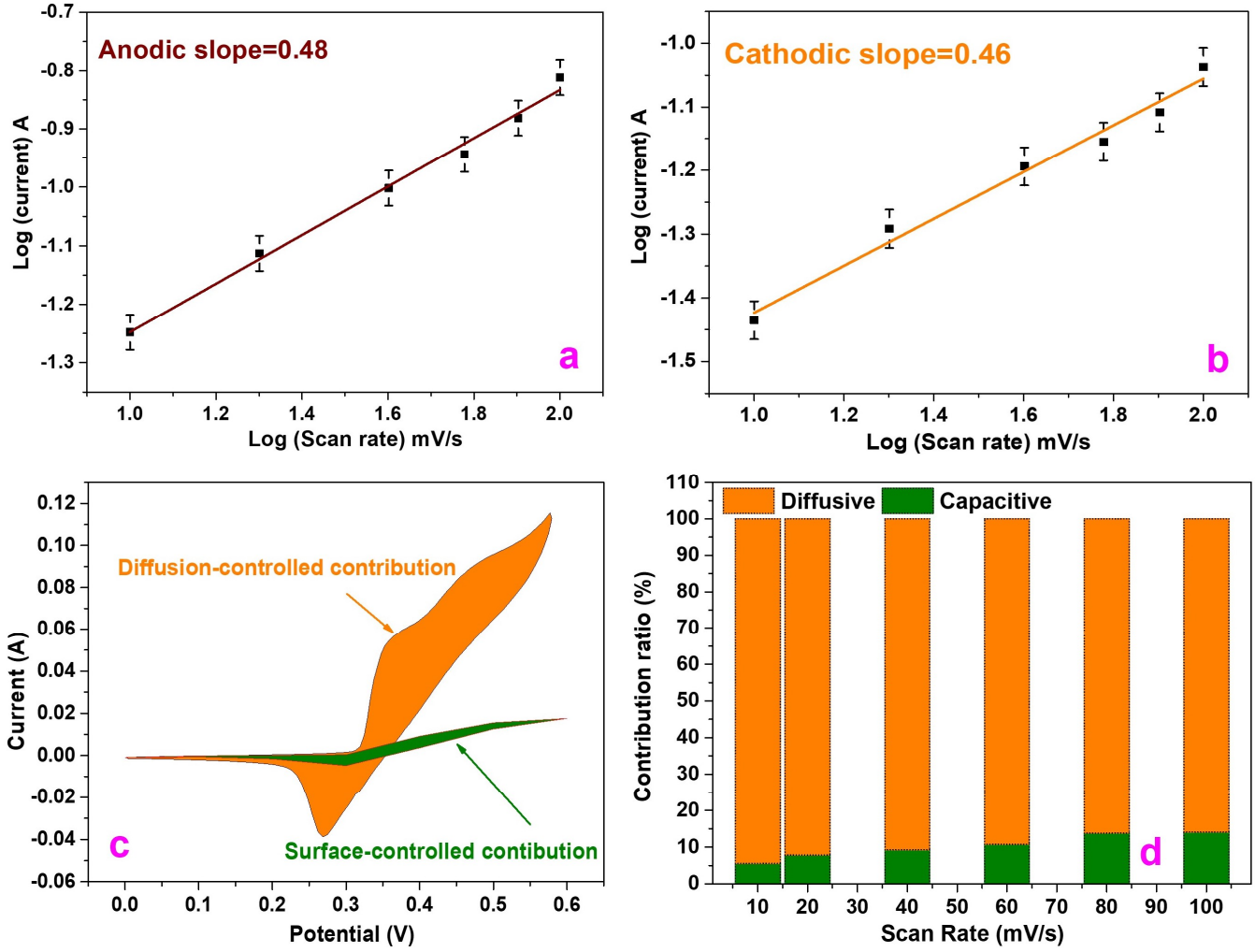

Figure 7. (**a**) Plot of log scan rate v/s log peak current for the anodic peaks of NPS1 nanocomposite SC electrode; (**b**) plot of log scan rate v/s log peak current for the cathodic peaks of NPS1; (**c**) CV curve obtained at a constant scan rate of 40 mV/s depicting the charge storage contributions from both diffusion-controlled and surface-controlled reactions; (**d**) Histogram showing the contributions to total charge storage at different scan rates.

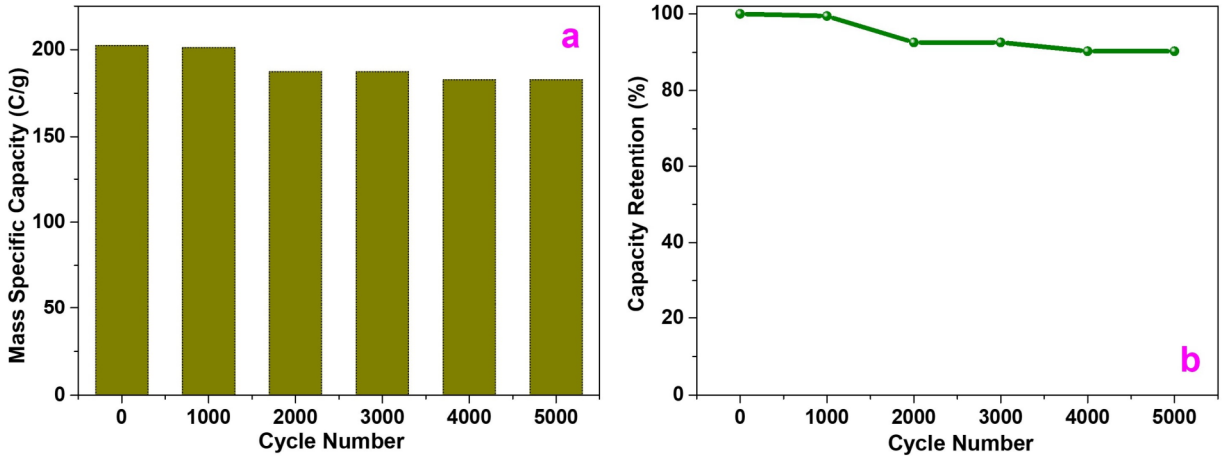

Figure 8. (**a**) Plot of variation in the mass specific capacitance of NPS1 nanocomposite SC electrode at different cycle numbers for 5000 cycles; (**b**) Plot of capacity retention of NPS1 nanocomposite SC electrode at different cycle numbers for 5000 cycles.

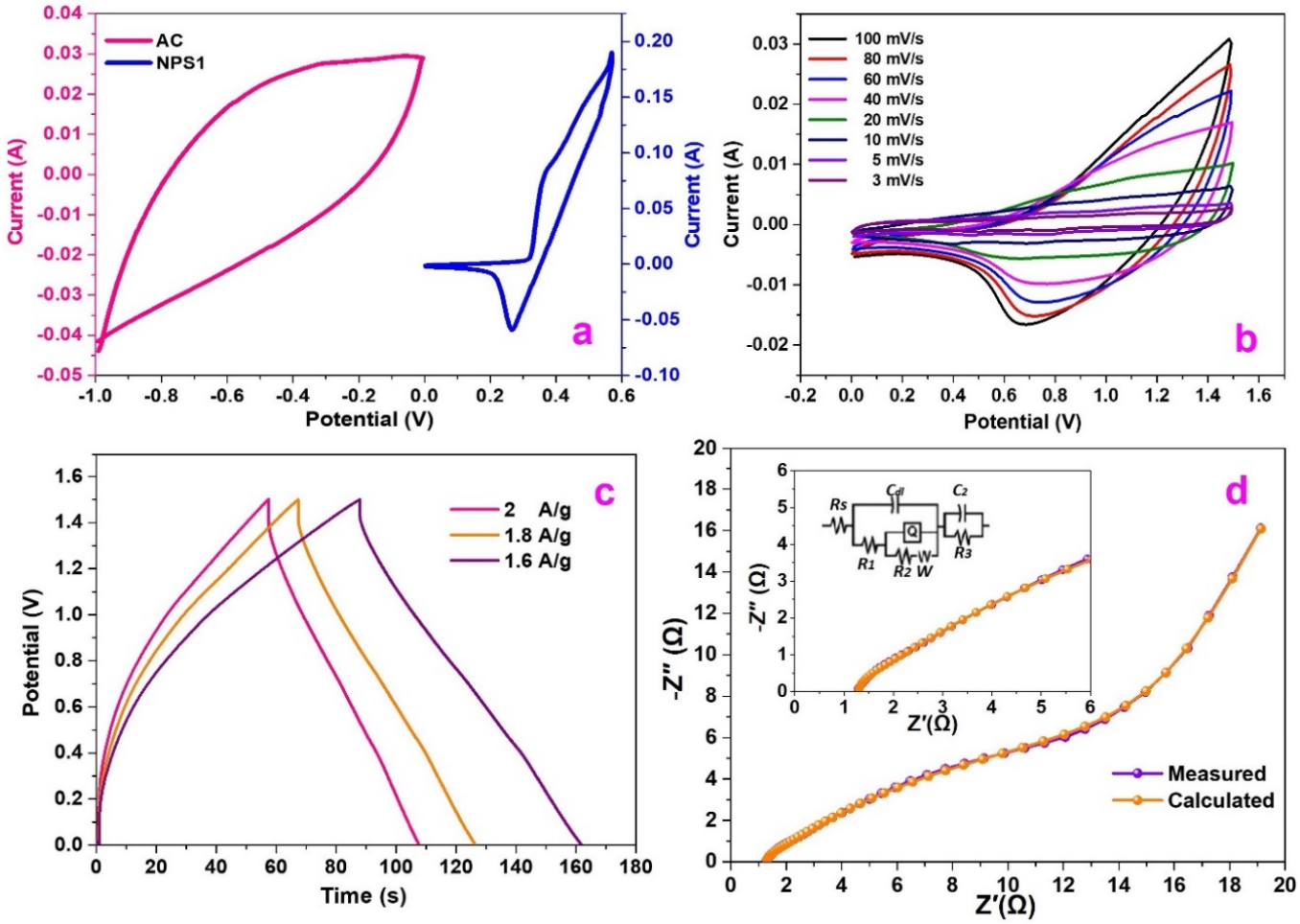

Figure 9. (**a**) CV curves obtained at a constant scan rate of 100 mV/s showing the different operating potential windows for AC and NPS1 electrodes; (**b**) CV curves obtained at different scan rates within a potential window of 0 to 1.5 V; (**c**) GCD curves of battery-type HSC cell obtained at different current densities; (**d**) Nyquist plot obtained for the battery-type HSC cell (Inset: Nyquist plot obtained in high-frequency region).

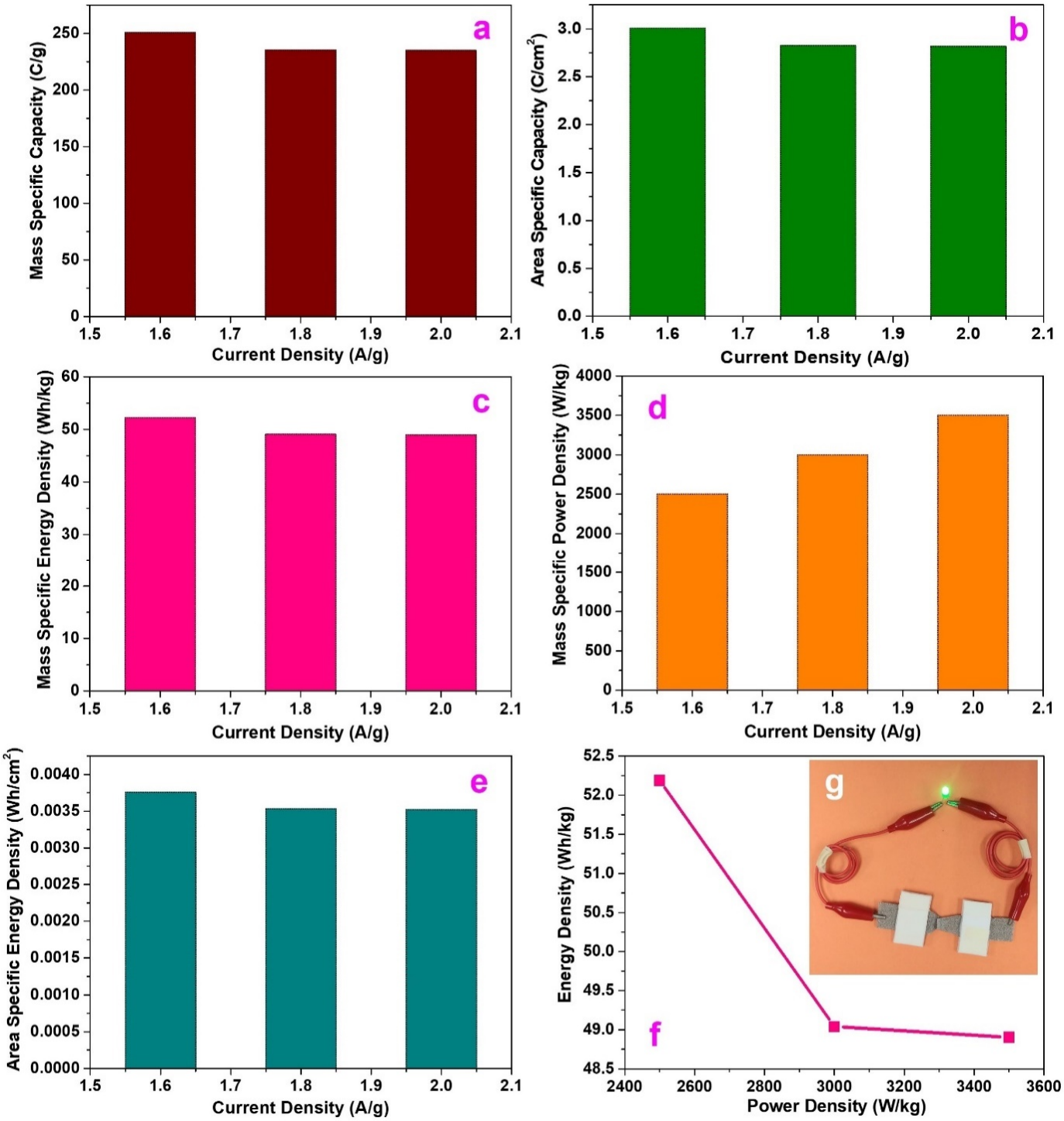

Figure 10. Electrochemical performance evaluation and device testing of the battery-type NPS1//AC HSC cell and module in 2 M KOH (aqueous) electrolyte. (**a**) Plot of variation in mass specific capacity (in C/g) with respect to current density; (**b**) Plot of variation in area specific capacity (C/cm^2) with respect to current density; (**c**) Plot of variation in mass specific energy density (in Wh/kg) with respect to current density; (**d**) Plot of variation in mass specific power density (W/kg) with respect to current density; (**e**) Plot of area specific energy density (in Wh/cm^2) with respect to current density; (**f**) Ragone plot for battery-type NPS1//AC HSC cell; (**g**) A battery-type NPS1//AC HSC module comprising of two similar battery-type NPS1//AC HSC cell prototypes connected in series lighting up a green LED immediately after charging it to 3 V.

The battery-type NPS1//AC HSC cell exhibits an area specific energy density of about 0.0037 Wh/cm^2 at a current density of 1.6 A/g. The variation in the area specific energy density with respect to current density is depicted in Figure 10e. The battery-type NPS1//AC HSC cell exhibits a mass specific power density of 2500 W/kg at a current density of 1.6 A/g and the variation in mass specific power density at different current densities is depicted in Figure 10d. The battery-type NPS1//AC HSC cell exhibits an area specific power density of 0.18 W/cm^2 at a current density of 1.6 A/g. A Ragone plot connecting the mass specific energy density and mass specific power density of battery-type NPS1//AC HSC cell is depicted in Figure 10f. A comparative analysis of the specific capacity, energy density, and power density of different transition metal sulfide/electronically conducting polymer nanocomposite SC electrodes is given in Table 1. From this Table, it can be observed that the present study is superior in terms of its energy density when compared to conducting polymers-based nanocomposite electrodes reported in the literature.

Table 1. Performance evaluation of sulfide with conducting polymer electrodes.

Transition Metal Sulfide/Conducting Polymer Nanocomposite SC Electrode	Synthesis Method	Morphology	Energy Density	Power Density	Ref.
MoS_2/PPy nanocomposite on reduced graphene oxide	Hydrothermal	Uniform and well-stacked structure	39.1 Wh/kg	0.70 kW/kg	[26]
MoS_2/PEDOT:PSS	Hydrothermal	Layered sheet-like structure	65.8 μWh/cm^2	0.5 mW/cm^2	[24]
NiS with PEDOT:PSS	Bar-coating approach	Chrysanthemum-like structure	24.52 Wh/kg	138.88 W/kg	[27]
PEDOT:PSS/rGO/MoS_2	Hydrothermal	Thin nanosheet	6.9 mWh/cm^3	173.6 mW/cm^3	[28]
MoS_2/PEDOT:PSS	Simple filtration	Nanosheets	4.9 mWh/cm^3	--	[29]
NiS_2@PEDOT:PSS	Slurry casting	2D Nanosheets	52.18 Wh/kg	2500 W/kg	* This work

* From the present comparison, it is clear that the prepared combination of NiS_2@ PEDOT:PSS exhibits higher energy and power density in comparison to others reported in the literature. Thus, it is clear that the as-synthesized NiS_2 with PEDOT:PSS combination have higher possibility to use in practical applications.

3.4. Electrochemical Performance Evaluation of NPS1/PEDOT:PSS//AC HSC Module

The practical application of NPS1 nanocomposite SC electrode was manifested by fabricating a battery-type NPS1//AC HSC module comprising of two similar battery-type NPS1//AC HSC cell prototypes connected in series in order to achieve a voltage of 3 V. The battery-type NPS1//AC HSC cell prototype was fabricated using NPS1 as positrode, AC as negatrode, Whatman® filter paper as electrolyte separator, and 2 M KOH (aqueous) electrolyte. The operation of the battery-type NPS1//AC HSC module was verified by lighting up a LED (operating voltage: 2.3–2.5 V). After charging the battery-type NPS1//AC HSC module to 3 V, it was connected to a green LED and lighting with high intensity was observed as shown in Figure 10g. From these results, it is clear that PEDOT:PSS incorporated into NiS_2 is an efficient electrode material for battery-type HSC fabrication.

4. Conclusions

The 2D NSN/PEDOT:PSS nanocomposite SC electrodes were prepared by the microwave-assisted hydrothermal method followed by slurry casting. Initially, NiS_2 with a sheet-like morphology was synthesized by the microwave-assisted hydrothermal method at 180 °C with a reaction time of 30 min. Further, 2D NSN/PEDOT:PSS nanocomposite electrodes were prepared by a facile slurry casting method. The microstructure and surface morphology of the best-performing 2D NSN/PEDOT:PSS nanocomposite (NPS1) were

examined using FESEM imaging. Among the various 2D NSN/PEDOT:PSS nanocomposite electrodes prepared (NPS1, NPS2, and NPS3), the best-performing one was NPS1 due to its open porous electrode architecture, which was found beneficial to obtain an excellent electrochemical performance. The battery-type SC electrode characteristics of the prepared NPS1 nanocomposite SC electrode were analyzed using Dunn's kinetic method and a capacitive (surface-controlled) contribution of 9.28% was estimated whereby the contribution from the diffusion-controlled process was 90.72% when calculated at a scan rate of 40 mV/s. The electrochemical cycling stability of the battery-type NPS1 nanocomposite SC electrode was evaluated and found to exhibit an excellent capacity retention of 90.11% even after completing 5000 cycles. To improve the charge storage performance of the 2D NSN for practical applications, an electronically conducting polymer, PEDOT:PSS, was incorporated by changing the concentration of NSN and PEDOT:PSS, and an optimal electrochemical performance was determined. A synergistic effect of a 3D architecture possessed by the NPS1 nanocomposite SC electrode consisting of a NSN with a 2D layered sheet-like structure along with the conducting wrapping of highly redox-active PEDOT:PSS is responsible for the enhanced charge storage. The NPS1 nanocomposite SC electrode exhibited a high mass specific capacity of 462.57 C/g at a scan rate of 10 mV/s. To demonstrate the potential of NPS1 nanocomposite SC electrode for practical device application, a battery-type HSC cell was fabricated using NPS1 as a positrode and AC as negatrode. The battery-type NPS1//AC HSC cell exhibited a mass specific capacity of 250.5 C/g at a current density of 1.6 A/g. The NPS1//AC HSC cell also exhibited a mass specific energy density of 52.18 Wh/kg with a corresponding power density of 2500 W/kg at a current density of 1.6 A/g. This higher performance exhibited by the NPS1 SC electrode was attributed to the synergistic effects of NiS_2 as well as the incorporation of highly redox-active PEDOT:PSS with it. A battery-type NPS1//AC HSC module comprising of two similar battery-type NPS1//AC HSC cell prototypes connected in series combination in order to achieve a voltage of 3 V was also fabricated and tested by lighting up a green LED with an operating voltage of 2.3–2.5 V.

Author Contributions: Conceptualization, S.A.T.; methodology, S.A.T.; software, S.A.T.; validation, S.A.T., J.C. and D.N.R.; formal analysis, S.A.T. and J.C.; investigation, S.A.T. and J.C.; resources, J.C. and D.N.R.; data curation, S.A.T.; writing—original draft preparation, S.A.T.; writing—review and editing, S.A.T., J.C. and D.N.R.; visualization, S.A.T., J.C. and D.N.R.; supervision, D.N.R.; project administration, J.C. and D.N.R. All authors have read and agreed to the published version of the manuscript.

Funding: This research received no external funding.

Institutional Review Board Statement: Not applicable.

Informed Consent Statement: Not applicable.

Data Availability Statement: All data used for this work are made available in this research.

Acknowledgments: The authors acknowledge Sunway University, Selangor, Malaysia for providing the necessary experimental facilities (including chemicals, materials and characterizations) for this research work.

Conflicts of Interest: The authors declare no conflicts of interest.

References

1. Krishnan, S.G.; Archana, P.; Vidyadharan, B.; Misnon, I.I.; Vijayan, B.L.; Nair, V.M.; Gupta, A.; Jose, R. Modification of capacitive charge storage of TiO_2 with nickel doping. *J. Alloys Compd.* **2016**, *684*, 328–334. [CrossRef]
2. Krishnan, S.G.; Reddy, M.; Harilal, M.; Vidyadharan, B.; Misnon, I.I.; Ab Rahim, M.H.; Ismail, J.; Jose, R. Characterization of $MgCo_2O_4$ as an electrode for high performance supercapacitors. *Electrochim. Acta* **2015**, *161*, 312–321. [CrossRef]
3. Molahalli, V.; Chaithrashree, K.; Singh, M.K.; Agrawal, M.; Krishnan, S.G.; Hegde, G. Past decade of supercapacitor research–lessons learned for future innovations. *J. Energy Storage* **2023**, *70*, 108062. [CrossRef]
4. Dutta, A.; Mahanta, J.; Banerjee, T. Supercapacitors in the light of solid waste and energy management: A review. *Adv. Sustain. Syst.* **2020**, *4*, 2000182. [CrossRef]

5. Zhao, B. Three-dimensional hybrid nanostructures of Fe_3O_4 nanoparticles/vertically-aligned carbon nanotubes for high-performance supercapacitors. *Electrochem* **2022**, *3*, 507–519. [CrossRef]
6. Thomas, S.A.; Cherusseri, J. Boron carbon nitride (BCN): Emerging two-dimensional nanomaterial for supercapacitors. *J. Mater. Chem. A* **2023**, *11*, 23148–23187. [CrossRef]
7. Krishnan, S.G.; Pham, H.D.; Mahale, K.; Nanjundan, A.K.; Dubal, D. Nanostructure-dependent electrochemical properties of Nb_2O_5 for long-life Li-ion batteries. *ACS Appl. Eng. Mater.* **2022**, *1*, 469–476. [CrossRef]
8. Wang, L.; Zhang, X.; Ma, Y.; Yang, M.; Qi, Y. Supercapacitor performances of the MoS_2/CoS_2 nanotube arrays in situ grown on Ti plate. *J. Phys. Chem. C* **2017**, *121*, 9089–9095. [CrossRef]
9. Kirti, R.G.; Divesh, N.S. A biodegradable polymer-based plastic chip electrode as a current collector in supercapacitor application. *Electrochem* **2022**, *3*, 379–396. [CrossRef]
10. Krishnamoorthy, K.; Veerasubramani, G.K.; Radhakrishnan, S.; Kim, S.J. Supercapacitive properties of hydrothermally synthesized sphere like MoS_2 nanostructures. *Mater. Res. Bull.* **2014**, *50*, 499–502. [CrossRef]
11. Thomas, S.A.; Cherusseri, J.; Rajendran, D.N. Rapid synthesis of hierarchical cobalt disulfide nanostructures by microwave-assisted hydrothermal method for high performance supercapatteries. *ACS Appl. Electron. Mater.* **2024**, *6*, 4321–4335. [CrossRef]
12. Harilal, M.; Krishnan, S.G. Nanocarbons and electric double-layer capacitors. In *Supercapacitors*; Elsevier: Amsterdam, The Netherlands, 2024; pp. 17–43.
13. Krishnan, S.G.; Harilal, M.; Jagadish, P. Ceramic-polyaniline composites for asymmetric supercapacitors. In *Surface Modification and Functionalization of Ceramic Composites*; Elsevier: Amsterdam, The Netherlands, 2023; pp. 371–396.
14. An, C.; Zhang, Y.; Guo, H.; Wang, Y. Metal oxide-based supercapacitors: Progress and prospectives. *Nanoscale Adv.* **2019**, *1*, 4644–4658. [CrossRef] [PubMed]
15. Hou, S.; Lian, Y.; Xu, Z.; Wang, D.; Ban, C.; Zhao, J.; Zhang, H. Construction of ball-flower like NiS_2@ MoS_2 composite for high performance supercapacitors. *Electrochim. Acta* **2020**, *330*, 135208. [CrossRef]
16. Iqbal, M.F.; Ashiq, M.N.; Zhang, M. Design of metals sulfides with carbon materials for supercapacitor applications: A review. *Energy Technol.* **2021**, *9*, 2000987. [CrossRef]
17. Thomas, S.A.; Cherusseri, J. Strategically designing layered two-dimensional SnS_2-based hybrid electrodes: A futuristic option for low-cost supercapacitors. *J. Energy Chem.* **2023**, *85*, 394–417. [CrossRef]
18. Krishnan, S.G.; Arunachalam, A.; Jagadish, P. Applications of supercapattery. In *Advances in Supercapacitor and Supercapattery*; Elsevier: Amsterdam, The Netherlands, 2021; pp. 311–348.
19. Dai, Z.; Xue, L.; Zhang, Z.; Gao, Y.; Wang, J.; Gao, Q.; Chen, D. Construction of single-phase nickel disulfide microflowers as high-performance electrodes for hybrid supercapacitors. *Energy Fuels* **2020**, *34*, 10178–10187. [CrossRef]
20. Yang, X.; Zhao, L.; Lian, J. Arrays of hierarchical nickel sulfides/MoS_2 nanosheets supported on carbon nanotubes backbone as advanced anode materials for asymmetric supercapacitor. *J. Power Sources* **2017**, *343*, 373–382. [CrossRef]
21. Reddy, B.J.; Vickraman, P.; Justin, A.S. Asymmetric supercapacitor device performance based on microwave synthesis of N-doped graphene/nickel sulfide nanocomposite. *J. Mater. Sci.* **2019**, *54*, 6361–6373. [CrossRef]
22. Shi, H.; Liu, C.; Jiang, Q.; Xu, J. Effective approaches to improve the electrical conductivity of PEDOT:PSS: A review. *Adv. Electron. Mater.* **2015**, *1*, 1500017. [CrossRef]
23. Fan, Z.; Ouyang, J. Thermoelectric properties of PEDOT:PSS. *Adv. Electron. Mater.* **2019**, *5*, 1800769. [CrossRef]
24. Chao, Y.; Ge, Y.; Chen, Z.; Cui, X.; Zhao, C.; Wang, C.; Wallace, G.G. One-pot hydrothermal synthesis of solution-processable MoS_2/PEDOT:PSS composites for high-performance supercapacitors. *ACS Appl. Mater. Interfaces* **2021**, *13*, 7285–7296. [CrossRef] [PubMed]
25. Thomas, S.A.; Cherusseri, J.; Rajendran, D.N. 2D nickel sulfide electrodes with superior electrochemical thermal stability along with long cyclic stability for supercapatteries. *Energy Technol.* **2024**, *12*, 2301641. [CrossRef]
26. Hao, J.; Liu, H.; Han, S.; Lian, J. MoS_2 nanosheet-polypyrrole composites deposited on reduced graphene oxide for supercapacitor applications. *ACS Appl. Nano Mater.* **2021**, *4*, 1330–1339. [CrossRef]
27. Punnoose, D.; Bae, J.-H.; Durga, I.K.; Thulasi-Varma, C.V.; Naresh, B.; Subramanian, A.; Raman, V.; Kim, H.-J. Preparation and electrochemical performances of NiS with PEDOT:PSS chrysanthemum petal like nanostructure for high performance supercapacitors. *Electrochim. Acta* **2017**, *254*, 269–279.
28. Zhou, Q.; Lv, G.; Wang, X.; Teng, W.; Hu, P.; Du, Y.; Li, H.; Hu, Y.; Liu, W.; Wang, J. Constructing a hierarchical ternary hybrid of PEDOT:PSS/rGO/MoS_2 as an efficient electrode for a flexible fiber-shaped supercapacitor. *ACS Appl. Energy Mater.* **2023**, *6*, 5797–5805. [CrossRef]
29. Ge, Y.; Jalili, R.; Wang, C.; Zheng, T.; Chao, Y.; Wallace, G.G. A robust free-standing MoS_2/poly (3,4-ethylenedioxythiophene): Poly (styrenesulfonate) film for supercapacitor applications. *Electrochim. Acta* **2017**, *235*, 348–355. [CrossRef]